View metadata, citation and similar papers at core.ac.uk
brought to you by CORE
provided by Caltech Authors - Main

Mon. Not. R. Astron. Soc. **325,** 412–418 (2001)

Tests for primordial non-Gaussianity

Licia Verde,[1★] Raul Jimenez,[2★] Marc Kamionkowski[3★] and Sabino Matarrese[4★]

[1]*Department of Astrophysical Sciences, Princeton University, Princeton, NJ 08540–1001, USA*
[2]*Department of Physics and Astronomy, Rutgers University, 136 Frelinghuysen Road, Piscataway, NJ 08854–8019, USA*
[3]*Mail Code 130–33, California Institute of Technology, Pasadena, CA 91125, USA*
[4]*Dipartimento di Fisica 'Galileo Galilei', via Marzolo 8, I-35131 Padova, Italy*

Accepted 2001 February 23. Received 2001 February 2; in original form 2000 November 13

ABSTRACT

We investigate the relative sensitivities of several tests for deviations from Gaussianity in the primordial distribution of density perturbations. We consider models for non-Gaussianity that mimic that which comes from inflation as well as that which comes from topological defects. The tests we consider involve the cosmic microwave background (CMB), large-scale structure, high-redshift galaxies, and the abundances and properties of clusters. We find that the CMB is superior at finding non-Gaussianity in the primordial gravitational potential (as inflation would produce), while observations of high-redshift galaxies are much better suited to find non-Gaussianity that resembles that expected from topological defects. We derive a simple expression that relates the abundance of high-redshift objects in non-Gaussian models to the primordial skewness.

Key words: methods: analytical – galaxies: clusters: general – cosmic microwave background – cosmology: theory – large-scale structure of Universe.

1 INTRODUCTION

Now that cosmic microwave background (CMB) experiments (Balbi et al. 2000; de Bernardis et al. 2000; Jaffe et al. 2001; Lange et al. 2001) have verified the inflationary predictions of a flat Universe and structure formation from primordial adiabatic perturbations, we are compelled to test further the predictions of the simplest single-scalar-field slow-roll inflation models and to look for possible deviations. Measurements of the distribution of primordial density perturbation afford such tests. If the primordial perturbations are entirely due to quantum fluctuations in the scalar field responsible for inflation (the 'inflaton'), then their distribution should be *very* close to Gaussian (e.g. Guth & Pi 1982; Starobinski 1982; Bardeen, Steinhardt & Turner 1983; Falk, Rangarajan & Srednicki 1993; Gangui 1994; Gangui et al. 1994; Gangui & Martin 2000; Wang & Kamionkowski 2000). However, multiple-scalar-field models of inflation allow for the possibility that a small fraction of primordial perturbations is produced by quantum fluctuations in a second scalar field. If so, the distribution of these perturbations could be non-Gaussian (e.g. Allen, Grinstein & Wise 1987; Kofman & Pogosyan 1988; Salopek, Bond & Bardeen 1989; Linde & Mukhanov 1997; Peebles 1999a,b; Salopek 1999). Moreover, it is still possible that some components of primordial perturbations are due to topological defects or some other exotic causal mechanism (Bouchet et al. 2000), and if so, their distribution should be non-Gaussian (e.g. Vilenkin 1985; Vachaspati 1986; Hill, Schramm & Fry 1989; Turok 1989; Albrecht & Stebbins 1992). Detection of any non-Gaussianity would thus be invaluable for appreciating the nature of the ultrahigh-energy physics that gave rise to primordial perturbations. Ruling such exotic possibilities in or out will also be necessary to test the assumptions that underly the new era of precision cosmology.

There are several observables that can be used to look for primordial non-Gaussianity. CMB maps probe cosmological fluctuations when they are closest to their primordial form, and many authors have developed various mathematical tools to test the Gaussian hypothesis. The statistics of the present-day large-scale structure (LSS) in the Universe can also be used (e.g. Coles et al. 1993; Luo & Schramm 1993; Lokas et al. 1995; Chodorowski & Bouchet 1996; Stirling & Peacock 1996; Durrer et al. 2000; Verde & Heavens 2000). The properties and abundances of the most massive and/or highest-redshift objects in the Universe also contain precious information about the nature of the initial conditions (e.g. Chiu, Ostriker & Strauss 1998; Matarrese, Verde & Jimenez 2000, hereafter MVJ00; Robinson, Gawiser & Silk 2000; Willick 2000; Verde et al. 2000b). In Verde et al. (2000a, hereafter VWHK00), the relative sensitivities of the CMB and LSS to several broad classes of primordial non-Gaussianity were compared, and it was found that the forthcoming CMB maps can provide more sensitive probes of primordial non-Gaussianity than galaxy surveys. Here we extend the results of that paper to include comparisons to the abundances of high-redshift galaxies as well as the abundance and

★E-mail: lverde@astro.princeton.edu (LV); rauj@physics.rutgers.edu (RJ); kamion@tapir.caltech.edu (MK); matarrese@pd.infn.it (SM)

© 2001 RAS

Downloaded from https://academic.oup.com/mnras/article-abstract/325/1/412/959797 by California Institute of Technology user on 19 May 2020

properties of clusters. One of our original aims was to determine whether any of these probes would be able to detect the miniscule deviations from Gaussianity that arise from quantum fluctuations in the inflation; unfortunately, we have not been able to find any. Nevertheless, some detectable deviations from Gaussianity are conceivable with multiple-field models of inflation and/or some secondary contribution to primordial perturbations from topological defects. We will follow VWHK00 and parametrize the primordial non-Gaussianity with a parameter that can be dialled from zero (corresponding to the Gaussian case) for two different classes of non-Gaussianity. We will then compare the smallest value for the parameter that can be detected with each of the different approaches.

2 THE METHOD

2.1 Models for primordial non-Gaussianity

There are infinite types of possible deviations from Gaussianity, and it is unimaginable to address all of them. However, we can consider plausible physical mechanisms that produce small deviations from the Gaussian behaviour and thus analyse the following two models for the primordial non-Gaussianity (e.g. Coles & Barrow 1987; MVJ00; VWHK00). In the first model, we suppose that the fractional density perturbation $\delta(\boldsymbol{x})$ is a non-Gaussian random field that can be written in terms of a Gaussian random field $\phi(\boldsymbol{x})$ using (Model A)

$$\delta = \phi + \epsilon_{\rm A}(\phi^2 - \langle\phi^2\rangle). \tag{1}$$

In the second model, we assume that the primordial gravitational potential $\Phi(\boldsymbol{x})$ is a non-Gaussian random field that can be written in terms of a Gaussian random field $\phi(\boldsymbol{x})$ using (Model B)

$$\Phi = \phi + \epsilon_{\rm B}(\phi^2 - \langle\phi^2\rangle). \tag{2}$$

Non-Gaussianity in the density field is then obtained from that in the potential through the Poisson equation. Here, Φ and δ refer to the primordial gravitational potential and density perturbation, respectively, before the action of the transfer function that takes place near the matter–radiation equality.

Although not fully general, these models may be considered as the lowest-order terms in Taylor expansions of more general fields, and are thus quite general for small deviations from Gaussianity. The scale-dependence of the non-Gaussianity in the two models differs. Model A produces deviations from Gaussianity that are roughly scale-independent on large scales, while Model B produces deviations from non-Gaussianity that become larger at larger distance scales. Although we choose these models essentially in an ad hoc way, the non-Gaussianity of Model B is precisely that arising in standard slow-roll inflation and in non-standard (e.g. multifield) inflation (Fan & Bardeen 1992; Falk et al. 1993; Gangui et al. 1994; Luo 1994; see also below). Model A more closely resembles non-Gaussianity than would be expected from topological defects (e.g. VWHK00). In either case, the lowest-order deviations from non-Gaussianity (and those expected generically to be the most easily observed) are the three-point correlation function (including the skewness, its zero-lag value) or equivalently the bispectrum, its Fourier-space counterpart. It is straightforward to calculate these quantities for both Models A and B.

2.2 Cosmic microwave background and large-scale structure

Temperature fluctuations in the CMB come from density perturbations at the surface of the last scatter, so the distribution of temperature fluctuations reflects that in the primordial density field. It is thus straightforward to relate the density-field bispectra of Models A and B to the bispectrum of the CMB. Density perturbations in the Universe today grow via gravitational infall from primordial perturbations in the early Universe, and this process alters the mass distribution in a calculable way. The cosmological perturbation theory allows the bispectrum for the mass distribution in the Universe today to be related to that for the primordial distribution.

VWHK00 calculated the smallest values of $\epsilon_{\rm A}$ and $\epsilon_{\rm B}$ which would be accessible with the CMB and with LSS. For the CMB calculation, it was assumed that a temperature map could be measured to the cosmic-variance limit only for multipole moments $\ell \lesssim 100$; it was assumed (quite conservatively) that no information would be obtained from larger multipole moments. The LSS calculations were made under the very optimistic assumption that the distribution of mass could be determined precisely from the galaxy distribution (i.e., that there was no biasing) in a survey of the size of the Sloan Digital Sky Survey (SDSS) and/or the Anglo-Australian Two-Degree Field Survey (2dF). VWHK00 found that the smallest values of ϵ that can be detected with the CMB under these assumptions is $\epsilon_{\rm A} \sim 10^{-2}$ and $\epsilon_{\rm B} \sim 20$ (Komatsu & Spergel 2001, including noise and foreground but neglecting dust contamination found that $\epsilon_{\rm B} \gtrsim 5$ from the Planck experiment), while the smallest values measurable with LSS are $\epsilon_{\rm A} \sim 10^{-2}$ and $\epsilon_{\rm B} \sim 10^3$. More realistically, the galaxy distribution will be biased relative to the mass distribution, and this will degrade the sensitivities to non-zero $\epsilon_{\rm A}$ and $\epsilon_{\rm B}$ obtainable with LSS. VWHK00 thus concluded that the CMB will provide a better probe on primordial non-Gaussianity for the class of models considered.

2.3 High redshift and/or massive objects

According to the Press–Schechter theory, the abundance of high redshift and/or massive objects is determined by the form of the high-density tail of the primordial density distribution function. A probability distribution function (PDF) that produces a larger number of $> 3\sigma$ peaks than a Gaussian distribution will lead to a larger abundance of rare high redshift and/or massive objects. Since small deviations from Gaussianity have a deep impact on those statistics that probe the tail of the distribution (e.g. Fry 1986, MVJ00), rare high-redshift and/or massive objects should be powerful probes of primordial non-Gaussianity. The number densities of high-redshift galaxies and/or of clusters (at either low or high redshifts) provide a very sensitive probe of the PDF. Since the Gaussian tail is decaying exponentially at higher densities, even a small deviation from Gaussianity can lead to huge enhancements in the number densities.

The non-Gaussianity parameters $\epsilon_{\rm A,B}$ are effectively 'tail enhancement' parameters (c.f. MVJ00).[1]

In order to determine the minimum value of $\epsilon_{\rm A,B}$ that can be

[1] In fact, when looking on a particular scale, it is always possible to parametrize the deviation of the PDF from Gaussianity, with some 'effective' $\epsilon_{\rm A}$ or $\epsilon_{\rm B}$, if the PDF is not too non-Gaussian. It is easy to understand this statement if one thinks in terms of skewness. Physical mechanisms that produce non-Gaussianity generically produce non-zero skewness in the PDF for the simple reason that an underdense region cannot be more empty than voids while overdense regions can become arbitrarily overdense. Skewness can be scale dependent, but for a given value of the skewness there is a one-to-one correspondence to the $\epsilon_{\rm A,B}$ parameters (see the Appendix).

Downloaded from https://academic.oup.com/mnras/article-abstract/325/1/412/959797 by California Institute of Technology user on 19 May 2020

detected using high-redshift objects, one needs to compute by how much the observed number density of objects changes with respect to the Gaussian case, when the primordial field is described by equations (1) and (2). We calculate this enhancement using the results for the mass function for mildly non-Gaussian initial conditions obtained analytically in MVJ00. Conservatively, we make the assumption that objects form at the same redshift at which they are observed ($z_c = z$); since for some objects the dark halo would have collapsed before we observe them, the assumption therefore gives a *lower limit* to the amount of non-Gaussianity.

The directly observed quantity, however, is not the mass function, but is $N(\geq M, z)$, the total number of objects – in the survey area – of mass $\geq M$ that collapse at redshift z. In fact it is extremely difficult to obtain an accurate estimate of the mass of high-redshift objects – what is a more robust quantity is the minimum mass that these objects must have in order to be detected at that redshift. This quantity is related to the mass function, $n(M, z)$, by

$$N(\geq M, z) = \int_M^\infty n(M, z)\,\mathrm{d}M. \tag{3}$$

In calculating the enhancement of high-redshift objects due to primordial non-Gaussianity, we restrict ourselves to consider, at any given redshift, only those masses $M \leq M_{\max}(z)$ for which at least one object is expected in the whole sky for Gaussian initial conditions [$N(\geq M_{\max}, z) = 1$ in 4π rad].[2] This is illustrated in Fig. 1 for a ΛCDM model [hereafter we adopt the currently favoured cosmological model with parameters $\Omega_0 = 0.3$, $\Lambda_0 = 0.7$, $h = 0.65$, $\sigma_8 = 0.99$ and the transfer function of Sugiyama (1995) with $\Omega_b = 0.015/h^2$] where the shaded region encloses predictions for $M_{\max}(z)$ from different mass functions (e.g. Press & Schechter 1974; Lee & Shandarin 1998; Sheth & Tormen 1999; Jenkins et al. 2001).

Given the rapidly dying tail of the Gaussian PDF, small uncertainties in the mass determination of high-redshift objects could lead to an overestimation of the value of $\epsilon_{\mathrm{A,B}}$. An overabundance of galaxies of estimated mass M_e, which in principle can be attributed to a non-zero value of $\epsilon_{\mathrm{A,B}}$, can also be explained under the hypothesis of Gaussian initial conditions if the actual galaxy mass M_{true} satisfies the condition $M_{\mathrm{true}} < M_e$. We thus include conservative values for the uncertainty ΔM in the mass determination of high-redshift objects, and we then calculate the minimum change ΔN in the number density of objects over the Gaussian case that cannot be attributed to the uncertainty in the mass determination. For a given uncertainty in the mass, this can be computed by using the standard Press–Schechter (PS) theory (Press & Schechter 1974). Observationally it is difficult to measure

[2] This choice for the threshold $N(\geq M_{\max}, z) = 1$ is motivated by the following considerations. Of course it is not robust to detect non-Gaussianity that suppresses the number of objects with respect to the Gaussian prediction, since one can always argue that one did not look hard enough, or that the objects are there but are somewhat 'invisible'. So we set to detect non-Gaussianity that enhances the number of objects relative to the Gaussian case. If within Gaussian initial conditions we expect $N(> M, z) \sim 0$ in the whole sky, and observations find $N(> M, z) > 1$ in the survey area, we can say that we have detected non-Gaussianity. However, the non-Gaussianity (or tail enhancement) parameter is directly related to the ratio of observed $N_{\mathrm{ng}}(> M, z)$ to the Gaussian predicted $N(> M, z)$ (see equation 4). Obviously this ratio is well defined for any $N_{\mathrm{ng}} > 0$ and $N > 0$, but the observed N_{ng} can only be an integer ≥ 1. The tail enhancement parameter will then make $N_{\mathrm{ng}} \geq N$ (and we consider only cases where $N_{\mathrm{ng}} \gtrsim 10N$). It is reasonable therefore to consider only those masses and redshifts for which the theoretical prediction for the Gaussian $N$is ≥ 1.

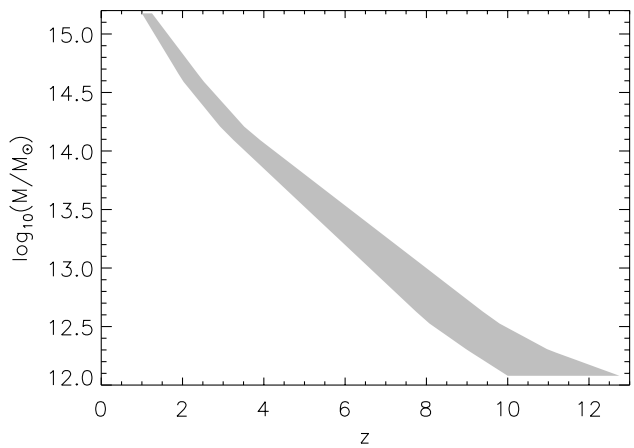

Figure 1. $M_{\max}$ as a function of redshift. At a given redshift one should only consider those masses ($\leq M_{\max}$) for which at least one object is expected in the whole sky for Gaussian initial conditions. The shaded region encloses predictions for $M_{\max}(z)$ from different mass functions in the literature; we adopted the currently favoured cosmological model with parameters: $\Omega_0 = 0.3$, $\Lambda_0 = 0.7$, $h = 0.65$, $\sigma_8 = 0.99$ and transfer function of Sugiyama (1995) with $\Omega_b = 0.015h^{2-1}$ (ΛCDM).

the mass of high-redshift clusters with an accuracy better than 30 per cent, using either weak lensing or the X-ray temperature, and of high-redshift galaxies better than a factor of 2 ($\Delta M = M$; at least of their stellar mass). Although the calculations in this section are obtained using the standard PS theory, our conclusions will be essentially unchanged if we had used modified PS theories (e.g. Lee & Shandarin 1998; Sheth & Tormen 2001; Sheth, Mo & Tormen 1999; Jenkins et al. 2001; see below).

With the mass uncertainties discussed above, we obtain that the minimum ΔN that cannot be attributed to ΔM is a factor of 10 for clusters and a factor of 100 for galaxies (see, e.g. fig. 6 of MVJ00).

We therefore estimate the minimum $\epsilon_{\mathrm{A,B}}$ that can be measured from the abundance of high-redshift galaxies and clusters as the one that corresponds respectively to a factor of 100 and 10 change in the observed number density of objects [$N(\geq M, z)$] over the Gaussian case. This condition can be written as

$$N_{\mathrm{ng}}(\geq M, z)/N(\geq M, z) \equiv R(M, z) \geq R_*, \tag{4}$$

where N is obtained using the Gaussian mass function while N_{ng} is obtained using the non-Gaussian mass function as in MVJ00, and R_* is set to be 100 for galaxies and 10 for clusters.

For small primordial non-Gaussianity (i.e. for small values of $\epsilon_{\mathrm{A,B}}$), it is possible to derive an expression for $R(M, z)$ using the analytical approximation for the mass function n_{ng} found in MVJ00. Doing so we find,

$$R(M, z) \simeq \frac{\int_M^\infty (\sigma_M M)^{-1} \exp\left[-\dfrac{\delta_*^2(z_c)}{2\sigma_M^2}\right] F(M, z_c, \epsilon_{\mathrm{A,B}})\,\mathrm{d}M}{\int_M^\infty (\sigma_M M)^{-1} \exp\left[-\dfrac{\delta_c^2(z_c)}{2\sigma_m^2}\right] \left|\dfrac{\mathrm{d}\sigma_M}{\mathrm{d}M}\right| \mathrm{d}M.} \tag{5}$$

Here,

$$F(M, z_c, \epsilon_{\mathrm{A,B}}) = \left| \frac{\delta_c(z_c)}{6\sqrt{1 - S_{3,M}\delta_c(z_c)/3}} \frac{\mathrm{d}S_{3,M}}{\mathrm{d}M} + \frac{\sqrt{1 - S_{3,M}\delta_c(z_c)/3}}{\sigma_M} \frac{\mathrm{d}\sigma_M}{\mathrm{d}M} \right|, \tag{6}$$

Downloaded from https://academic.oup.com/mnras/article-abstract/325/1/412/959797 by California Institute of Technology user on 19 May 2020

and

$$\delta_*(z_c) = \delta_c(z_c)\sqrt{1 - S_{3,M}\delta_c(z_c)/3}, \tag{7}$$

$$\delta_c(z_c) = \Delta_c/D(z_c), \tag{8}$$

where $D(z_c)$ is the linear-theory growth factor, and Δ_c is the linear extrapolation of the overdensity for spherical collapse.

In the formulae above, $S_{3,M}$ denotes the primordial skewness,

$$S_{3,M} = \epsilon_{A,B}\mu^{(1)}_{3,M}/\sigma^2_M, \tag{9}$$

where the expressions for $\mu^{(1)}_{3,M}$ and σ^2_M can be found in MVJ00 section 3.2, equations (37) and (38). However, for $S_3 \gtrsim 1/\delta_c(z_c)$, the mass function $n_{ng}(M, z)$ has to be evaluated numerically and equation (5) is not valid.

For the cosmological model considered here and the redshifts of interest, the quantity Δ_c takes a nearly constant value ($\approx$1.686) in the PS theory. A better fit to the mass function of halos in high-resolution *N*-body simulations is, however, obtained by lowering Δ_c for rare objects and giving it an extra mass and redshift dependence (Sheth & Tormen 1999; Bode et al. 2001), as motivated by ellipsoidal collapse (e.g. Lee & Shandarin 1998; Sheth, Mo & Tormen 1999).

It is possible to understand the effect of a lower Δ_c by the following argument. For rare fluctuations such as high-redshift objects, one is probing the mass function above the knee. Since the mass function drops very rapidly as M increases, we can approximate $N(> M, z_c) \sim n(M, z_c)M$. It is then possible to obtain an analytic expression for $r(M, z_c) \equiv n_{ng}(M, z_c)/n(M, z_c) \sim R(M, z_c)$ if the primordial non-Gaussianity is small,

$$r(M, z_c) \simeq \exp\left[\frac{\Delta_c^3 S_3}{6\sigma_M^2}\right]\left|\frac{\delta_c}{6\sqrt{1 - \frac{S_3\delta_c}{3}}}\frac{dS_3}{d\sigma_M} + \sqrt{1 - \frac{S_3\delta_c}{3}}\right|. \tag{10}$$

For a given mass M, r (M, z_c) slowly decreases on lowering Δ_c, slightly damping the effect of non-Gaussianity. For example, when lowering Δ_c from the value 1.686 that we assume here, to the value $\approx$1.5 – appropriate to fit the numerical mass function of Sheth & Tormen (1999) for the range of masses and redshifts considered here – $r(M, z_c)$ decreases by less than a factor of 2. However this effect is compensated by the fact that, by lowering Δ_c, objects are created more easily also with Gaussian initial conditions, and it is therefore possible to consider objects of higher M and/or z, where the effect of non-Gaussianity is bigger. In summary, the conclusions obtained by assuming $\Delta_c = 1.686$ will not be substantially modified.

It is important to note that for Model A, the primordial skewness has the same sign as ϵ_A, while for Model B it has the opposite sign of that of ϵ_B. In detecting non-zero $\epsilon_{A,B}$ from CMB maps, the sign of the skewness does not influence the accuracy of the detection of non-Gaussianity, but when using the abundance of high-redshift objects the sign of the skewness matters. Only a positively skewed primordial distribution will generate more high-redshift objects than that predicted in the Gaussian case. Although a negatively skewed probability distribution will generate fewer objects than the Gaussian case, it might be difficult to attribute a decrement exclusively to a negatively skewed distribution. Therefore in the following we will consider only negative ϵ_B and positive ϵ_A.

2.3.1 *Cluster size–temperature distribution*

Verde et al. (2000b) showed that the size–temperature (ST) distribution of clusters is fairly sensitive to the degree of primordial non-Gaussianity. If clusters are created from rare Gaussian peaks, the spread in formation redshift should be small and so should the scatter in the ST distribution. Conversely, if the PDF has long non-Gaussian tails, then clusters of a given mass that we observe today should have a broader redshift formation distribution and thus a broader ST relation. In Verde et al. (2000b), the non-Gaussianity considered is a lognormal distribution; it is not strictly equivalent to Models A or B considered here. However, for small deviations from Gaussianity, the two models can be identified if, for a given scale, they produce the same skewness in the density fluctuation field. We thus find that in the ΛCDM model the minimum ϵ_A and ϵ_B detectable with the ST distribution method are 3×10^{-3} and 500, respectively. These estimates assume that the cosmology and σ_8 are well known, but use only the local cluster data set of Mohr et al. (2000). Of course, with improved observational data, the ST method could probably yield stronger constraints.

3 RESULTS

Table 1 summarizes our results.

We find that the non-Gaussianity of Model A has a greater effect on high-redshift galaxies than on high-redshift clusters. This can be understood for the following reason. For Model A the skewness $S_{3,M}$ is approximately scale independent ($dS_{3,M}/dM = 0$). Thus, as found in MVJ00, the mass function for non-Gaussian initial conditions is obtained from the PS mass function for Gaussian initial conditions replacing $\delta_c(z_c) \rightarrow \delta_*(z_c)$. The effect of a non-zero skewness is therefore to lower the effective threshold for collapse, thus allowing more objects to be created. For a given S_3, $\delta_*(z_c)$ is a monotonically decreasing function of z_c. Since galaxies can be observed at z_c much bigger than that of clusters, the effect is greater. On the other hand, clusters are better probes than galaxies for Model B. In fact, for Model B the induced skewness in the density field is scale dependent and the effect of non-Gaussianity is roughly the same for galaxies with $8 < z < 10$ and clusters with $1 < z < 3$. However, since mass determinations are more accurate for clusters than for galaxies, we have $R_{*,\text{clusters}} < R_{*,\text{galaxies}}$: clusters are therefore better probes.

In Fig. 2 we show the ratio $R = N_{ng}(\geq M, z)/N(\geq M, z)$ [cf.

Table 1. Minimum $|\epsilon_A|$ and $|\epsilon_B|$ detectable form different observables and their sign when positive skewness is required for detection. For Model A the primordial skewness has the same sign as ϵ_A, while for Model B the primordial skewness has the opposite sign as ϵ_B. In detecting non-zero $\epsilon_{A,B}$ from CMB maps, the sign of the skewness does not influence the accuracy of the detection of non-Gaussianity, but, when using the abundance of high-redshift objects it is robust to detect non-Gaussianity that produces an excess rather than a defect in the number density. Only a positively skewed primordial distribution will generate more high-redshift objects than predicted in the Gaussian case.

Observable	Min. $\lvert\epsilon_A\rvert$	Min. $\lvert\epsilon_B\rvert$
CMB	$10^{-3} \sim 10^{-2}$	20
LSS	10^{-2}	$10^3 \sim 10^4$
High-z obj.	$(+)5 \times 10^{-4}$ (gal.)	$(-)$ 200 (clusters)
ST relation	$(+)3 \times 10^{-3}$	$(-)$ 500

Downloaded from https://academic.oup.com/mnras/article-abstract/325/1/412/959797 by California Institute of Technology user on 19 May 2020

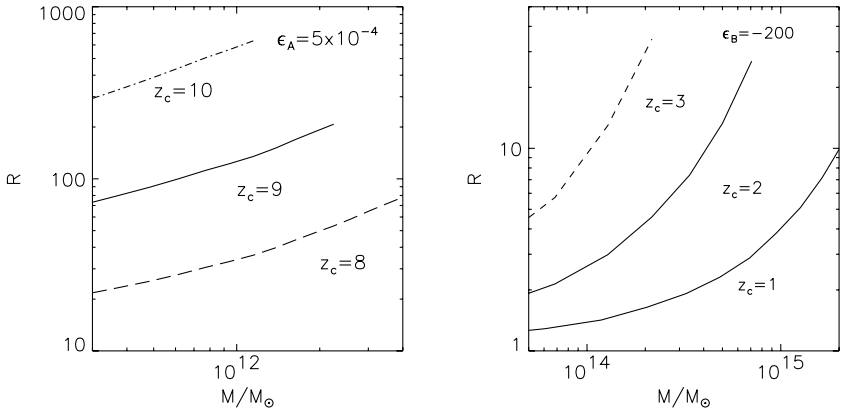

Figure 2. Ratio $R(M, z) = N_{\rm ng}(\geq M, z)/N(\geq M, z)$ for galaxies at redshift $z = 8$–10 for $\epsilon_{\rm A} = 5 \times 10^{-4}$ (left panel) and clusters at redshift $z = 1$–3 for $\epsilon_{\rm B} = 200$ (right panel), as a function of M. Lines are plotted only for masses where, for Gaussian initial conditions, one would expect to observe at least one object in the whole sky with the most conservative estimate (see Fig. 1). Note that these high-redshift objects represent 3 to 5σ peaks. The values for the number density enhancement R that can be safely attributed to primordial non-Gaussianity are $R = 100$ for galaxies (left panel) and $R = 10$ for clusters (right panel). See text for details.

equation (5)] for galaxies at redshift $z = 8$–10 for $\epsilon_{\rm A} = 5 \times 10^{-4}$ (Model A, left panel) and clusters at redshift $z = 1$–3 for $\epsilon_{\rm B} = -200$ (Model B, right panel), as a function of M. Lines are plotted only for masses where, for Gaussian initial conditions, one would expect to observe at least one object in the whole sky with the most conservative estimate (see Fig. 1). Note that those high-redshift objects represent 3 to 5σ peaks. If we now require $R(M, z_{\rm c}) > R_*$, we deduce that the minimum detectable deviation from Gaussian initial conditions will be $\epsilon_{\rm A} \sim 5 \times 10^{-4}$ (from high-redshift galaxies) and $|\epsilon_{\rm B}| \sim 200$ (from high-redshift clusters). We also estimate that an uncertainty of 10 per cent on σ_8 would propagate into an uncertainty of 25 per cent in $\epsilon_{\rm B}$ (from clusters) and of 70 per cent in $\epsilon_{\rm A}$ (from galaxies).

The minimum $\epsilon_{\rm B}$ detectable from high-redshift cluster abundances is much larger than the value that can be measured from the CMB ($\epsilon_{\rm B} \sim 5$ to 20 for Planck data), while for $\epsilon_{\rm A}$, high-redshift galaxies are much better probes than the CMB, which can only detect $\epsilon_{\rm A} \sim 10^{-2}$.

We therefore conclude that if future Next Generation Space Telescope (NGST) or 30- to 100-m ground-based telescope observations of high-redshift galaxies yield a significant number of galaxies at $z \sim 10$ and are able to determine their masses within a factor of 2, these observations will perform better than CMB maps in constraining primordial non-Gaussianity of the form of Model A with positive $\epsilon_{\rm A}$. Conversely, forthcoming CMB maps will constrain deviations from Gaussianity in the initial conditions much better than observations of high-redshift objects for Model B (with positive *and* negative value for $\epsilon_{\rm B}$) and for Model A with negative $\epsilon_{\rm A}$.

3.1 Slow-roll parameters and primordial skewness

The type of non-Gaussianity of Model B is particularly interesting because initial conditions set from standard inflation show deviations from Gaussianity of this kind. In fact, it is possible to relate the two slow-roll parameters,

$$\epsilon_* = \frac{m_{\rm Pl}^2}{16\pi}\left(\frac{V'}{V}\right)^2, \quad \text{and} \quad \eta_* = \frac{m_{\rm Pl}^2}{8\pi}\left[\frac{V''}{V} - \frac{1}{2}\left(\frac{V'}{V}\right)^2\right], \tag{11}$$

to the non-Gaussianity parameter $\epsilon_{\rm B}$. In equation (11) $m_{\rm Pl}$ is the Planck mass, V denotes the inflation potential and V' and V'' are the first and second derivatives with respect to the scalar field. The skewness S_3 for $\Phi_{\rm B}$, $S_{3,\Phi} = \langle\Phi_{\rm B}^3\rangle/\langle\Phi_{\rm B}^2\rangle^2$, can be evaluated following a similar calculation of Buchalter & Kamionkowski (1999), obtaining

$$S_{3,\Phi} = 2\epsilon_{\rm B} \times 3[1 + \gamma(n)], \tag{12}$$

where $\gamma(n) \ll 1$ and weakly depends on n if $n < 0$, but diverges for $n > 0$. For a scale-invariant matter–density power spectrum, $n = -3$, $\gamma(n) = 0$, and so $S_{3,\Phi} = 6\epsilon_{\rm B}$.

We can then compare this expression with the value for the skewness parameter for the gravitational potential arising from inflation to infer the magnitude of $\epsilon_{\rm B}$. Gangui et al. (1994) calculate the CMB skewness for the Sach–Wolfe effect S_2 in several inflationary models; S_2 is related to $S_{3,\Phi}$ by $S_2 = S_{3,\Phi}{\rm A}_{\rm sw}^{-1}$ where ${\rm A}_{\rm sw} = 1/3$. From this it follows that $S_2 = 3S_{3,\Phi} = 18\epsilon_{\rm B}$. The condition for slow roll from Gangui et al. (1994) is $S_2 \leq 20$; thus, $\epsilon_{\rm B} \leq 1$, and the relation with the slow-roll parameters is (cf. Wang & Kamionkowski 2000)

$$\epsilon_{\rm B} = (5/2)\epsilon_* - (5/3)\eta_*. \tag{13}$$

Since this combination of the slow-roll parameters is different from the combination that gives the spectral slope n of the primordial power spectrum ($n = 2\epsilon_* - 6\eta_* + 1$), in principle, if $\epsilon_{\rm B}$ could be measured with an error $\ll 1$, it would be then possible to determine the shape of the inflation potential through equation (11). However, from the present analysis, an error of $\epsilon_{\rm B}$ of about an order of magnitude larger seems to be realistically achievable.

4 DISCUSSION AND CONCLUSIONS

We considered two models for small primordial non-Gaussianity, one in which the primordial density perturbation contains a term that is the square of a Gaussian field (Model A), and the other in which the primordial gravitational potential perturbation contains a term proportional to the square of a Gaussian (Model B). The non-Gaussianity of Model B is precisely that arising in standard slow-roll inflation and in non-standard inflation, while Model A more closely resembles the non-Gaussianity that would be expected from topological defects. We investigated the relative sensitivities of several observables for testing for deviations from Gaussianity: CMB, LSS and high redshift and/or massive objects (e.g. galaxies and clusters).

The analytic tools developed above allow us to address the question of whether the abundance of currently known high-redshift

Downloaded from https://academic.oup.com/mnras/article-abstract/325/1/412/959797 by California Institute of Technology user on 19 May 2020

objects can be accommodated within the framework of inflationary models for a given cosmology. Recently Willick (2000) has studied in detail the mass determination of the cluster MS1054-03 concluding that its mass lies in the range $1.4 \pm 0.3 \times 10^{15}$ M for $\Omega_m = 0.3$ [similar to the independent mass estimates by, e.g. Newmann & Arnaud (2000) and Tran et al. (2000)]. As already pointed out by Willick (2000), for $\Omega_m \geq 0.3$ the expected number of objects like MS1054-03 in the survey area is ≤ 0.01; i.e. it must be a 3σ fluctuation or larger. Using the formalism we have described here, a primordial non-Gaussianity parametrized by $\epsilon_B \geq 400$ would be required to account for MS1054-03 as a 1σ fluctuation in the ΛCDM model described above. This value is much too large to be consistent with the slow-roll inflation. Our calculation shows that if such a non-Gaussianity exists, it would be easily detectable from the forthcoming CMB maps.

ACKNOWLEDGMENTS

LV and RJ thank the Caltech theoretical astrophysics group for hospitality. MK was supported in part by NSF AST-0096023, NASA NAG5-8506, and DoE DE-FG03-92-ER40701.

REFERENCES

Albrecht A., Stebbins A., 1992, Phys. Rev. Lett., 68, 2121
Allen T. J., Grinstein B., Wise M. B., 1987, Phys. Lett. B, 197, 66
Balbi A. et al., 2000, ApJ, 545, L1
Bardeen J. M., Steinhardt P. J., Turner M. S., 1983, Phys. Rev. D, 28, 679
Bode P., Bahcall N. A., Ford E. D., Ostriker J., ApJ, 2001, ApJ, 551, 15
Bouchet R., Peter P., Riazuelo A., Sakellariadou M., 2000 (astro-ph/0050220)
Buchalter A., Kamionkowski M., 1999, ApJ, 521, 1
Chiu W. A., Ostriker J., Strauss M. A., 1998, ApJ, 494, 479
Chodorowski M. J., Bouchet F. R., 1996, MNRAS, 279, 563
Coles P., Moscardini L., Lucchin F., Matarrese S., Messina A., 1993, MNRAS, 264, 740
Coles P., Barrow J. D., 1987, MNRAS, 228, 407
de Bernardis P. et al., 2000, Nat, 404, 955
Durrer R., Juskiewicz R., Kunz M., Uzan J., 2000, Phys. Rev. D, 6205335
Falk T., Rangarajan R., Srednicki M., 1993, ApJ, 403, L1
Fan Z., Bardeen J. M., 1992, University of Washington preprint, UW-PT-92-11
Fry N. J., 1986, ApJ, 308, L71
Gangui A., 1994, Phys. Rev. D, 50, 3684
Gangui A., Martin J., 2000, MNRAS, 313, 323
Gangui A., Lucchin F., Matarrese S., Mollerach S., 1994, ApJ, 430, 447
Guth A., Pi S.-Y., 1982, Phys. Rev. Lett., 464, L11
Hill C. T., Schramm D. N., Fry J. N., 1989, Comments Nucl. Part. Phys., 19, 25
Jaffe A. H. et al., 2001, Phys. Rev. L, 86, 3475
Jenkins A., Frenk C. S., White S. D. M., Colberg J. M., Cole S., Evrard A. E., Yoshida N., 2001, MNRAS, 321, 372
Kofman L., Pogosyan D. Y., 1988, Phys. Lett. B, 214, 508
Komatsu E., Spergel D., 2001, Phys. Rev. D, 630, f61a
Lange A. E. et al., 2001, Phys. Rev. D, 630, e411
Lee J., Shandarin S. F., 1998, ApJ, 500, 14
Linde A. D., Mukhanov V., 1997, Phys. Rev. D, 56, 535
Lokas E. L., Juszkiewicz R., Weinberg D. H., Bouchet F. R., 1995, MNRAS, 274, 744
Luo X., 1994, ApJ, 427, L71
Luo X., Schramm D. N., 1993, ApJ, 408, 33
Matarrese S., Verde L., Jimenez R., 2000, ApJ, 541, 10, (MVJ00)
Mohr J. J., Reese E. D., Ellingson E., Lewis A. D., Evrard A. E., 2000, 544, 109
Newmann D. M., Arnaud M., 2000, ApJ, 542, 35
Peebles P. J. E., 1999a, ApJ, 510, 523
Peebles P. J. E., 1999b, ApJ, 510, 531
Press W. H., Schechter P., 1974, ApJ, 187, 425
Robinson J., Gawiser E., Silk J., 2000, ApJ, 532, 1
Salopek D., 1999, AIP Conf. Proc., 478, 180
Salopek D., Bond J. R., Bardeen J. M., 1989, Phys. Rev. D, 40, 1753
Sheth R., Tormen G., 1999, MNRAS, 308, 119
Sheth R., Mo H. J., Tormen G., 2001, MNRAS, 323, 1
Starobinski A. A., 1982, Phys. Lett. B, 117, 175
Stirling A. J., Peacock J. A., 1996, MNRAS, 283, 99
Sugiyama N., 1995, ApJS, 100, 281
Tran K. H. et al., 2000, ApJ, 522, 39
Turok N., 1989, Phys. Rev. Lett., 63, 2625
Vachaspati T., 1986, Phys. Rev. Lett., 57, 1655
Verde L., Heavens A., 2001, ApJ, in press
Verde L., Wang L., Heavens A. F., Kamionkowski M., 2000a, MNRAS, 313, 141 (VWHK00)
Verde L., Kamionkowski M., Mohr J. J., Benson A. J., 2000b, MNRAS, 321, L7
Vilenkin A., 1985, Phys. Rep., 121, 263
Wang L., Kamionkowski M., 2000, Phys. Rev. D, 61, 063504
Willick J. A., 2000, ApJ, 530, 80

APPENDIX A

In this appendix we quote the expressions for the primordial bispectrum and skewness for the two non-Gaussian models considered in this paper. The LSS bispectrum for model A is (e.g. VWHK00)

$$B(\boldsymbol{k}_1, \boldsymbol{k}_2, \boldsymbol{k}_3) = 2\epsilon_A P(k_1)P(k_2) + cyc. \tag{A1}$$

where P denotes the power spectrum. The CMB bispectrum for model A is (e.g. VWHK00)

$$B_{\ell_1\ell_2\ell_3} \simeq \sqrt{\frac{(2\ell_1+1)(2\ell_2+1)(2\ell_3+1)}{4\pi}} \begin{pmatrix} \ell_1 & \ell_2 & \ell_3 \\ 0 & 0 & 0 \end{pmatrix} \times \frac{2\epsilon_A}{g}\left(\frac{2}{3}C_{\ell_1}C_{\ell_2}\frac{\ell_1^2\ell_2^2}{\ell_3^2} + cyc.\right) \tag{A2}$$

where C_ℓ denotes the CMB power spectrum, g denotes the radiation transfer function and (…) denotes the Wigner 3J symbol. The LSS bispectrum for model B is (e.g. VWHK00)

$$B(\boldsymbol{k}_1, \boldsymbol{k}_2, \boldsymbol{k}_3) \simeq \left[P(k_1)P(k_2)2\epsilon_B \frac{\mathcal{M}_{k_3}}{\mathcal{M}_{k_1}\mathcal{M}_{k_2}}\right] + cyc. \tag{A3}$$

where[3] $\mathcal{M}_k \sim [2k^2T(k)(1+z)]/(3H_0^3)$ and T denotes the matter transfer function. The CMB bispectrum for model B is (e.g. Luo 1994; VWHK00; Wang & Kamionkowski 2000; Komatsu & Spergel 2001):

$$B_{\ell_1\ell_2\ell_3} = \sqrt{\frac{(2\ell_1+1)(2\ell_2+1)(2\ell_3+1)}{4\pi}} \begin{pmatrix} \ell_1 & \ell_2 & \ell_3 \\ 0 & 0 & 0 \end{pmatrix} \times \frac{2\epsilon_B}{g}(C_{\ell_1}C_{\ell_2} + cyc.) \tag{A4}$$

The corresponding primordial skewness $S_3 = \langle\delta^3\rangle/\langle\delta^2\rangle^2$ where δ denotes $\delta\rho/\rho$ for the LSS case and $\Delta T/T$ for the CMB is easily obtained from the consideration that $\langle\delta^3\rangle$ is given by:

$$\langle\delta^3\rangle_{\rm LSS} = \int \frac{d^3k_1}{(2\pi)^3}\frac{d^3k_2}{(2\pi)^3} d^3k_3 B(\boldsymbol{k}_1, \boldsymbol{k}_2, \boldsymbol{k}_3)\delta^D(\boldsymbol{k}_1 + \boldsymbol{k}_2 + \boldsymbol{k}_3) \tag{A5}$$

[3] This expression is strictly valid only for an *Einstein* de Sitter universe. For a more general model $\mathcal{M}$ is defined by $\delta_k(z) = \mathcal{M}_k(z)\Phi(k)$ where Φ denotes the gravitational potential field.

Downloaded from https://academic.oup.com/mnras/article-abstract/325/1/412/959797 by California Institute of Technology user on 19 May 2020

(in the absence of spatial filtering) and

$$\langle\delta^3\rangle_{\rm CMB} = \frac{1}{4\pi}\sum_{\ell_1\ell_2\ell_3}\sqrt{\frac{(2\ell_1+1)(2\ell_2+1)(2\ell_3+1)}{4\pi}} \times \begin{pmatrix} \ell_1 & \ell_2 & \ell_3 \\ 0 & 0 & 0 \end{pmatrix} B_{\ell_1\ell_2\ell_3} \tag{A6}$$

for LSS and CMB, respectively. For example in the LSS, model A, for a power-law power spectrum and in the absence of spatial filtering[4] we have $S_3 = 6\epsilon_{\rm A}$.

This paper has been typeset from a TEX/LATEX file prepared by the author.

[4] The expression for $\langle\delta^3\rangle_{\rm LSS}$ in the general case can easily be derived following the calculations of Buchalter & Kamionkowski (1999) by setting $b_1 = 0$ and $b_2/2 = \epsilon_{\rm A}$.

Downloaded from https://academic.oup.com/mnras/article-abstract/325/1/412/959797 by California Institute of Technology user on 19 May 2020